ELSEVIER

Contents lists available at ScienceDirect

Journal of Molecular Liquids

journal homepage: www.elsevier.com/locate/molliq





Instantaneous fundamental modes and contact angles of droplets from surface atoms

Amal Kanta Giri a,b, Marcello Sega c,*

- ^a Khalisani Mahavidyalaya, University of Burdwan, Khalisani, Chandannagar, 712138-West Bengal, India
- ^b Department of Physics, University of Bayreuth, 95440 Bayreuth, Germany
- ^c Department of Chemical Engineering, University College London, WC1E 7JE, London, United Kingdom

ABSTRACT

Contact angle measurements of sessile or moving droplets are by far the most common way to characterize their wetting properties. The typical route to obtain contact angle estimates from atomistic molecular dynamics simulations requires the calculation of an isochore or the equimolar dividing surface, both of which need sizeable statistics to achieve acceptable accuracy and are less suitable in non-stationary conditions. Here, we propose an algorithm for estimating the contact angle that relies on the identification of interfacial molecules, which can determine the instantaneous location of the liquid surface. We apply this algorithm to calculate the contact angles of water droplets at equilibrium and out of equilibrium on graphite-like substrates, paying particular attention to modeling the presence of excited modes using general ellipses to fit the droplet surface. The algorithm is implemented in a user-friendly way in the Pytim software package.

1. Introduction

Contact angle measurement is a fundamental technique for estimating the wetting properties of solid surfaces by a liquid, providing essential insights into surface energies, adhesion, and wettability. Traditional experimental methods for contact angle measurement, such as the sessile drop [1] and Wilhelmy plate [2] techniques, provide macroscopic observations. Particle-based simulation measurements of contact angles [3–5], on the other hand, offer a microscopic perspective on static and dynamic wetting phenomena [6–8].

On rigid substrates, the Young-Duprè equation and its generalization to line tension [9] connect the contact angle to the balance of intermolecular forces at the substrate-liquid-vapor contact line, and its precise determination is pivotal for applications ranging from biomaterial coatings and self-cleaning surfaces to enhanced oil recovery and microfluidic devices. If the droplet is floating on another liquid, the angles at the contact line are determined by Neumann's law instead [10]. The liquid on a solid substrate is a particular case of the most general framework of deformable substrates [11]. Regardless of the theoretical framework describing the mechanics of wetting, the measurement of contact angles proves to be complicated by several factors both in experiments [12] and in simulations [13–15]. The goniometric approach requires identifying the surface of the liquid, typically by locating a liquid isochore or the local equimolar surface (see, e.g., [16,17]). This calculation inevitably requires sampling density profiles with the conse-

quent necessity of performing a time average (spatial average might be limited by size), reducing the usefulness of these approaches to equilibrium or stationary conditions and preventing the investigation of spatial correlation effects.

Because capillary waves smear the average density profiles of interfaces, it is often believed that the liquid-vapor interface of small molecular liquids is diffuse, with an impact on the strategies chosen to locate it [18]. However, far from the critical point, liquid/vapor interfaces of small molecular liquids have a width that is comparable with the molecular size [19] and retain, at least in part, the strong correlations that characterize the bulk [20].

The need for an instantaneous determination of the contact angle has been recognized before by Nezbeda and coworkers, who used an alpha-shape-based method [21], and later by Galindo and coworkers [22], who built on the Instantaneous Liquid Interfaces method of Willard and Chandler [23]. Willard and Chandler's method defines the location of the instantaneous liquid surface as a specific iso-density surface of the convolution of a Gaussian kernel with the positions of atomic centers.

Here, we use as an interface location method the Generalised Identification of Truly Interfacial Molecules (GITIM) [24,25], which we already successfully employed to investigate the dynamic wetting of droplets [26] and, which provides direct access to the instantaneous location of interfacial atoms, as shown in Fig. 1.

E-mail address: m.sega@ucl.ac.uk (M. Sega).

^{*} Corresponding author.

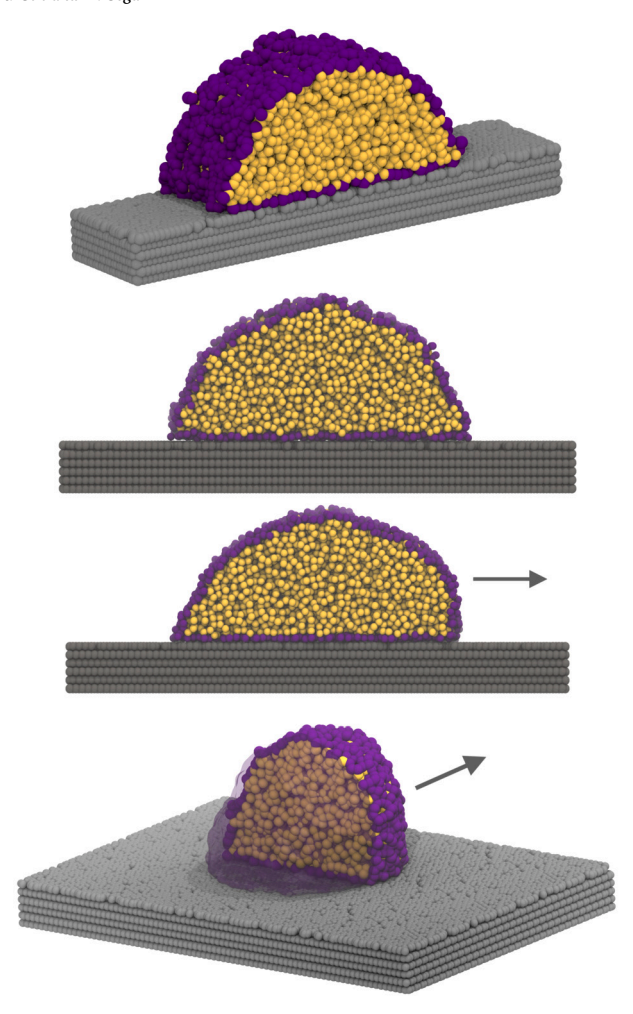


Fig. 1. Molecular dynamics simulations snapshots. From top to bottom, the first three panels show the cylindrical droplet in: equilibrium, oblique projection; equilibrium, x-z projection; stationary state x-z projection. Bottom panel: a spherical droplet pulled by an oblique force. The oxygen atoms of the droplet are shown in purple (surface oxygen atoms) and yellow (other oxygen atoms). The carbon atoms of the substrate are shown in gray. The arrow indicates the direction of the applied body force. In the bottom panel, part of the droplet atoms are replaced by a transparent surface to show a cross-section parallel to the x-z plane.

The average shape of a droplet surface at equilibrium, at least on scales larger than the substrate-liquid interaction range, is that of a spherical cap because surface tension acts towards minimizing the liquid-vapor interfacial area. Out of equilibrium, this is not true anymore, and one needs to resort to other approaches to take into account the presence of excited modes. Considering the excited modes is necessary even at equilibrium when analyzing instantaneous configurations because all surface modes are excited by thermal agitation, including the longest wavelength modes that deform the global shape of the droplet.

In other words, while high-frequency thermally activated modes appear as ripples on the surface of the droplet, the lowest frequency one contributes to the overall deformation of the droplet, which, even at equilibrium, will keep wobbling because of thermal agitation. As we will describe later, the lowest-frequency mode is an ellipsoidal deformation.

In the following, we will show how to access the contact angle of instantaneous configurations in three exemplary cases involving non-equilibrium simulations of droplets that are spanning (cylindrical) or not (deformed spherical caps) the periodic boundary conditions. Fitting the surface profile using an ellipse allows us to describe the long-wave

excited modes quite accurately, but the usual techniques based on linear least squares turned out to be unsuitable for the task.

2. Methods

2.1. Molecular dynamics simulations

In this work, we performed non-equilibrium molecular dynamics simulations of 7332 SPC/E water molecules [27,28] condensed on one side of a stack of six rigid graphene flakes, following the protocol developed in a previous publication [29]. We use two setups, one with flakes of size 19.8936 nm \times 4.6794 nm and the other with size 19.8936 nm × 14.0382 nm. In both cases, the flakes are separated by 0.335 nm along the normal direction, z, and fill the x - y cross-section of their corresponding simulation box with a z-edge length of 17 nm. We removed a random selection of carbon atoms from the first layer (about 35% of the first layer atoms) to generate a microscopically rough surface that could provide sizeable friction and prevent the appearance of a divergent slip length [30,29]. Note that although this surface has the structure of graphite, the interaction parameters have not been tuned to match specifically any wetting experimental results. In addition, it is worth noticing that the experimental measurement of contact angle on graphite reported in the literature suffers from a considerable spread, which has multiple origins, ranging from the presence of defects to that of hydrocarbon contamination [31]. Also, contact angle measurements of water droplet with comparable sizes are experimentally accessible, see, e.g., the review of Mendez-Vilas and coworkers [32].

In the first setup, shown in three panels at the top of Fig. 1, the water molecules are condensed in a droplet that spans the periodic boundary conditions along the y axis. In this way, the droplet has a cylindrical cap shape, often used in literature to avoid contact line contributions, and keep the contact angle independent on the droplet size [33]. In the second setup, shown in the bottom panel of Fig. 1, the droplet does not span the periodic boundary conditions and, at equilibrium, takes the shape of a spherical cap.

The code we developed for this occasion as a new observable implemented in the Pytim software [25]¹ and works both for cylindrical and spherical caps. Fig. 2 reports a simple usage example of the Pytim implementation of the observable for calculating the contact angles, which includes several routines for fitting, generating, and transforming between different representations of ellipses and ellipsoids. Internally, the code essentially does the following steps

- wrap the surface atoms positions to remove periodic boundary conditions effects
- 2. disregard atoms below the chosen elevation cut
- 3. perform a linear least square fit to obtain a first estimate of the parameters
- 4. use the output of the linear fit as initial values for the nonlinear least square
- ${\bf 5.}\,$ compute the contact angles from the analytical expression

All simulations were performed with the GROMACS simulation package [34], version 2018, using a timestep of 2 fs, the smooth Particle-Mesh-Ewald method [35,36] to treat the long-range contribution of electrostatics and dispersion forces [37,38]. The simulations are performed at constant temperature, using a modified Nosè-Hoover thermostat [39,40] (characteristic time, 1 ps, reference temperature 300 K) that is coupled only along the y direction, to retain thermodynamic consistency [41,42,26].²

Finally, we used the GITIM [24] method, as implemented in Pytim [25], to identify the surface molecules. GITIM works by performing

¹ http://github.com/Marcello-Sega/pytim.

² https://github.com/Marcello-Sega/gromacs/tree/decoupled-thermostat.

```
[1]: import pytim
     import MDAnalysis as mda
     from pytim.observables import ContactAngle
     from pytim.datafiles import *
     # use one of the test configurations provided with the package
     u = mda.Universe(WATER DROPLET CYLINDRICAL GRO)
     # define droplet and substrate
     droplet = u.select_atoms("name OW")
     substrate = u.select_atoms("name C")
     # compute the interfacial atoms
     inter = pytim.GITIM(universe=u,group=droplet, molecular=False,
                         alpha=2.5, cluster_cut=3.4)
     # instantiate the contact angle observable, with periodicity
     # along y, removing the center of mass along x, and disregarding
     # liquid phase atoms within the first 5.5 Angstrom from the substrate.
     CA = ContactAngle(inter, substrate,periodic=1,removeCOM=0,
                       contact_cut=5.5, bins=100)
     # sample the first configuration
     CA.sample()
     # report left and right last sampled contact angles
     CA.contact angles
[1]: [81.14385791250194, 82.99751791548044]
[2]: # report the last computed coefficients, updated with a call
     # to CA.contact_angles() or CA.fit_ellipse(), and the canonical
     # form with center (x0,y0), semiaxes (a,b), tilt angle phi and,
     # in addition, the eccentricity e
     CA.polynomial_coefficients, CA.canonical_form
[2]: (array([ 5.68316564e-01, -1.87448671e-02, 4.40058343e-01, 5.96136793e
              8.81318523e+00, -1.76407803e+03]),
      {'x0': -0.6898592236734848,
       'y0': -10.028348169762317,
       'a': 64.1560325515468.
       'b': 56.37686069780883,
       'phi': 1.4982353227415925,
       'e': 0.47728960354598277})
[3]: # Sample points from the ellipse, given the canonical form
     x,y = CA.ellipse(CA.canonical_form,npts=1000)
     x.shape, y.shape
[3]: ((1000,), (1000,))
```

Fig. 2. Usage example for the calculation of contact angles of a cylindrical droplet.

a Delaunay triangulation [43] of the molecular positions and labeling as interfacial molecules those at the edges of triangles large enough to host a probe sphere of a given size. The probe sphere radius determines the resolution at which the interface is described and can be chosen in such a way that the local position of the interface is compatible with the Gibbs equimolar dividing surface [44]. We have chosen this approach, as opposed to a continuum-based method like the Willard-Chandler one, to have direct access to the surface atoms, as this can be beneficial when calculating other properties including, for example, the velocity of surface atoms [26]. After obtaining the molecular coordinates from a molecular dynamics simulation and identifying water interfacial molecules using the GITIM algorithm, we determine the liquid-vapor interface by subtracting from the set of interfacial water molecules those in close contact with the substrate (i.e., closer than the first minimum of the carbon-oxygen radial distribution function). This

way, the procedure would work also for rough surfaces, not just flat ones like in the present case.

2.2. Ellipse and ellipsoid fitting

The next step requires processing the coordinates of the liquid-vapor interfacial atoms to measure the quantities that characterize the instantaneous geometry of the droplet, including the contact angle. When computing droplet profiles and contact angles of equilibrium droplets from averaged density profiles, the natural choice is to fit the data to a circumference arc or a spherical cap, as the spherical (and cylindrical, for infinitely long droplets or in the presence of periodic boundary conditions) shape minimizes the surface area. However, performing instantaneous measurements without a time average requires considering the presence of excited surface modes. For macroscopically flat surfaces, these modes are the usual thermal capillary waves characterized

by a continuum spectrum for an infinite surface. Instead, the modes of droplets need to be bound at long wavelengths because of their finite size. The normal modes of a spherical surface are, in general, divided between spheroidal vibrations ${}_{n}S^{l}$ and toroidal or torsional vibrations $_{n}T^{l}$ and labeled by the number of nodal intersections nalong the radial direction and l-1 along the surface. The n=0 modes are the fundamental ones, while n > 0 identifies overtones. For example, the ${}_{0}S^{0}$ mode corresponds to an isotropic expansion and contraction (a breathing mode), while the ${}_{0}S^{2}$ mode, with displacement field $\mathbf{s} = \sqrt{5/(16\pi)}U(r)(3\cos^2\theta - 1)\hat{\mathbf{r}} + \sqrt{15/(8\pi)}V(r)\sin\theta\cos\theta\,\hat{\boldsymbol{\theta}}$, is often described as an oscillation between an oblate and a prolate ellipsoid [45]. Unlike solids, liquids can not resist deformation in response to applied shear stress over time, so only spheroidal modes are relevant for a liquid droplet in the low frequency limit, and are represented by the Rayleigh-Lamb deformations [46], the lowest mode of which is the quadrupolar $Y_{20}(\theta) = \sqrt{15/(16\pi)}(3\cos^2\theta - 1)$, analogous to the spheroidal mode. While the eigenmodes of sessile droplets are much more complex and rich in phenomenology [47], it is an established practice to approximate the shape of droplets under shear with an ellipsoid [48,49]. This is not true only for droplets under shear, as the radial profile of a revolution ellipsoid, $r(\theta) = r_0 (1 - \epsilon^2 \cos^2 \theta)^{-1/2}$ can be approximated, for small eccentricities ϵ , as $r(\theta) \simeq r_0 + (r_0/2)\epsilon^2 \cos^2 \theta$, and so it can be used effectively to fit the spheroidal modes.

Here, we consider only the lowest frequency modes or shear-induced deformations, in the limit of small eccentricity. As both are approximated well by elliptical or ellipsoidal shapes, describing them requires an appropriate fitting procedure for ellipses and ellipsoids. For ellipses, the typical approach consists in translating the problem of fitting the quadratic form $F(x,y) = ax^2 + bxy + cy^2 + dx + ey + f = 0$ into the linear least squares problem of minimizing $|\mathbf{Dp}|^2$, where the $6 \times N$ design matrix $\mathbf{D} = [x_i^2, x_i y_i, y_i^2, x_i, y_i, 1]$ is defined by the set of N points (x_i, y_i) , and the vector of parameters is $\mathbf{p} = [a, b, c, d, e, f]$. In solving this problem, one has to avoid the trivial solutions and solutions that represent conics other than the ellipse. Fitzgibbon incorporated the ellipticity constraint $4ac - b^2 > 0$ in an elegant way [50], providing a simple and robust algorithm, which has proven extremely popular. The algorithm provides the polynomial coefficients \mathbf{p} as the eigenvector corresponding to the only positive eigenvalue λ of the generalized eigenvalue problem

$$\mathbf{D}^T \mathbf{D} \mathbf{p} = \lambda \mathbf{C} \mathbf{p},\tag{1}$$

where \mathbf{C} is a 6×6 matrix with zeros everywhere but along the antidiagonal of its first 3×3 block, which takes the value (-2,1,-2). In this work, we use a modified version of Fitzgibbon's linear least square algorithm, which improves its stability [51].

Despite their appealing simplicity and speed, these linear least squares approaches have the common problem of minimizing the algebraic rather than the geometric, or root mean square, distance (RMSD), which is what one would like to do for this problem. A simple test on points sampled from equilibrium simulations of a droplet shows that Fitzgibbon's best-fitting ellipse yields higher RMSD values than the best fit to an arc of circumference, which is problematic in the present context.

Thanks to its robustness, however, Fitzgibbon's algorithm or variants thereof like that of Halíř and Flusser [51], which we use here, is an excellent choice to select the initial guess for a subsequent nonlinear fit. In our implementation, we carry out the nonlinear fit using the Nelder-Mead algorithm to minimize the ellipse's RMSD, using a penalty function to avoid sets of parameters that do not satisfy the ellipticity constraint.

One further remark is in order. In performing the fit, we did not include the region of the droplet near the substrate (within a 5.5 Å region) to avoid measurement of the microscopic contact angle. This is a region that is one water molecule in size, where the distortion of the density profile due to the interaction with the substrate is so strong that it would introduce a large bias in the measurement of the contact

angle. As it is custom practice (see, e.g., the discussion in [22]) we exclude these molecules from the fit.

Finally, the contact angles of the ellipse can be calculated by solving the tedious but simple geometrical problem of finding the slopes m of the secant segments $y-y_1=m(x-x_1)$ with two coincident solutions, which pass through the points satisfying the ellipse equation F(x,y)=0 at a desired elevation y_1 , leading to $m=4acx_1y_1+2aex_1-b^2x_1y_1-bdx_1-bey_1-2bf+2cdy_1+de$, where x_1 can be easily found by solving $F(x_1,y_1)=0$ and is given by

$$2ax_1 = -by_1 - d \pm \sqrt{-4acy_1^2 - 4aey_1 - 4af + b^2y_1^2 + 2bdy_1 + d^2}.$$

Here, we have chosen the elevation to be that of the atomic centers in the topmost graphene flake.

For ellipsoids, instead, we employ the approach by Turner and coworkers [52] to perform the initial linear least squares fit. In this case, the design matrix is

$$\mathbf{D} = [x^2 + y^2 - 2z^2, x^2 - 2y^2 + z^2, 4xy, 2xz, 2yz, x, y, z, 1],$$

and the generalized eigenvalue to be solved is

$$\mathbf{D}^T \mathbf{D} \mathbf{p}' = \lambda \mathbf{D}^T \mathbf{E} \mathbf{p}', \tag{2}$$

with $\mathbf{E} = [x^2 + y^2 + z^2]$. The elements of the eigenvector

$$\mathbf{p}' = [u, v, m, n, p, q, r, s, t]^T$$

are related to the coefficients

$$\mathbf{p} = [a, b, c, f, e, d, g, h, k, l]^T$$

of the polynomial

$$ax^{2} + by^{2} + cz^{2} + 2fyz + 2gxz + 2hxy + px + qy + rz + d$$

by the relations

$$\mathbf{p} = [1 - u - v, 1 - u + 2v, 3 - a - b, -2m, -n, -p, -q, -r, -s, -t]^{T}.$$

The problem of generating points on the general ellipsoid can be solved by using the affine transformation (the ellipsoid is not necessarily centered in the origin)

$$\mathbf{r} = \mathbf{v} + \mathbf{T}\mathbf{s} \tag{3}$$

that maps the unit sphere centered in the origin,

 $\mathbf{s} = [\sin\theta\cos\phi, \sin\theta\sin\phi, \cos\theta]^T$

to the points on the ellipsoid, \mathbf{r} . The connection between the affine transformation and the coefficients of the polynomial can be found using another standard representation of the ellipsoid, namely,

$$(\mathbf{r} - \mathbf{v})^T \mathbf{A}' (\mathbf{r} - \mathbf{v}) = k^2. \tag{4}$$

It can be shown [53] that $T = kA'^{-1/2}$. It is important to use the representation with a generic value of the constant k instead of the more conventional choice, k = 1. In this way, the quadratic form has the same additional degree of freedom as the polynomial one, allowing us to proceed with a term-by-term comparison to identify the elements of the affine transformation. The polynomial can be recast in the matrix form

$$\mathbf{r}^T \mathbf{A} \mathbf{r} + \boldsymbol{\beta}^T \mathbf{r} + \gamma = 0, \tag{5}$$

with

$$\mathbf{A} = \begin{bmatrix} a & h & g \\ h & b & f \\ g & f & c \end{bmatrix}, \quad \boldsymbol{\beta} = [p, q, r]^T, \quad \gamma = d.$$
 (6)

After expansion and comparison, one finds $\mathbf{A}' = \mathbf{A}$, $\mathbf{v} = -1/2\mathbf{A}^{-1}\boldsymbol{\beta}$, and $k^2 = (1/4)\boldsymbol{\beta}^T\mathbf{A}^{-1}\boldsymbol{\beta} - \gamma$, allowing to determine the affine transformation given the polynomial coefficients.

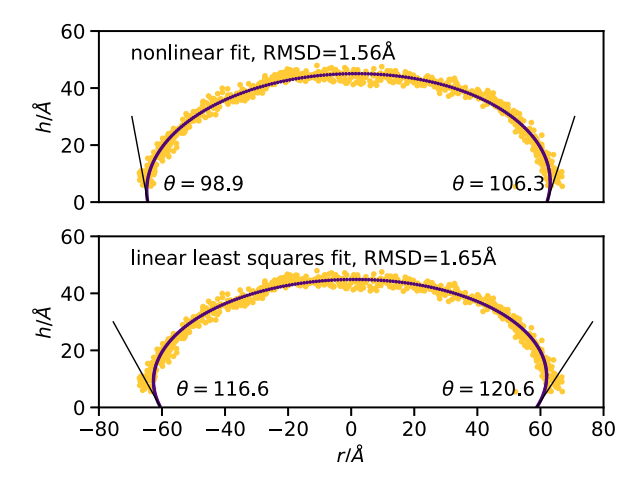


Fig. 3. Positions of the instantaneous surface molecules (points) and results of best fit (solid line) for a droplet in the stationary state in the presence of a downward acceleration (top panel: nonlinear fit procedure; bottom panel: fit using Fitzgibbon's algorithm).

The contact line is given by the (x,y) points solving the ellipsoid equation at the elevation of choice $z=z_1$. The analytical solution is that of an ellipse (the contact line) with parameters $\mathbf{p}_{\text{contact}}=[a,2h,b,2gz_1+p,2fz_1+q,rz_1+d]^T$. With $\mathbf{p}_{\text{contact}}$ at hand, one can generate points belonging to the contact line, remap them back onto the unit sphere with the inverse of the affine transformation, and compute the corresponding tangent vectors. Eventually, one needs to apply the affine transformation to obtain the tangent vectors on the ellipsoid and, from there, calculate the normal ones, from which one can easily read out the contact angle along the contact line.

It is worth noticing that the whole fitting procedure inclusive of the various geometrical transformations required is rather tedious, and the implementation with the Pytim package makes the process of obtaining the contact angles values straightforward for the user, as demonstrated by the few steps required by the user in Fig. 2.

3. Results and discussion

To test our approach, we start by calculating the properties of the average cylindrical droplet surface at equilibrium, focusing only later on the instantaneous surface. We sampled 500 frames, collecting the surface positions of surface oxygen atoms in a histogram. The histogram holds the information on the radial distance from the center of the droplet as a function of the azimuthal angle. In this way, we avoid the large variance close to the tip of the droplet that characterizes binning the elevation from the substrate. Note that cylindrical droplets also have capillary fluctuations along their axis spanning the periodic boundary conditions, but we don't consider them here, as they are always just fluctuating around zero.

The best fit through the binned surface atoms positions sampled over 500 frames of an equilibrium trajectory, for example, yielded an ellipse that is indistinguishable to the eye from the best fitting circumference, with RMSDs equal to 1.406 and 1.409 Å, respectively. The least-square algorithm solution, on the other hand, yields an RMSD of 1.474 Å, with visible differences close to the base of the droplet and a contact angle estimate of $84.5\pm1.0~{\rm deg}.$

Next, we analyze the instantaneous profile of a cylindrical droplet subject to a downward acceleration of $0.0025~\text{nm/ps}^2$ pointing towards the substrate. This acceleration induces a deformation of the droplet, which reaches a new stationary shape after a few tens of picoseconds. In Fig. 3, we show the result of the best fit according to the linear least squares algorithm (bottom panel) and the Nelder-Mead nonlinear optimization (top panel). The points represent the atomic positions of an instantaneous configuration of the liquid/vapor interfacial molecules.

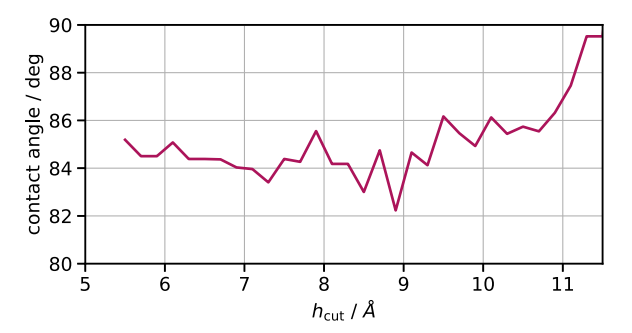


Fig. 4. Dependence of the contact angle (average between left and right measured from a single cylindrical droplet configuration at equilibrium), as a function of the cutoff elevation $h_{\rm cut}$ below which atoms are not considered for the fitting procedure.

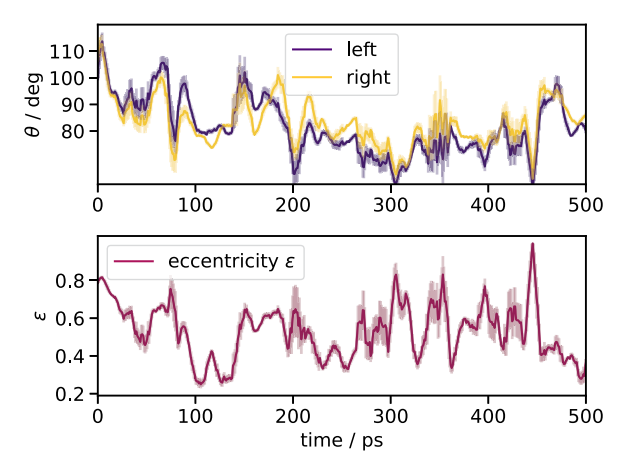


Fig. 5. Time evolution of left and right contact angles (top panel) and eccentricity (bottom panel) during the relaxation of the compressed droplet towards equilibrium. The shaded area represents one standard deviation.

The nonlinear fit is superior even by visual inspection, especially in the region close to the lower part of the droplet, and the lower RMSD value confirms this. Note that we used the same set of atoms to perform both fits. The fact that the least squares algorithm deviates more (in a geometrical sense) close to the base is because the linear least squares fit minimizes the algebraic distance $\sum_i |F(x_i,y_i)|^2$, and not the geometric one.

The question of the stability of this fit is also quite important. The elliptical fit is notoriously more sensitive to outliers than the circular fit. If we progressively exclude atoms closer to the substrate ones than a cutoff $h_{\rm cut}$, the measured contact angle of a single configuration sampled from equilibrium, shown in Fig. 4 is relatively stable from the lowest value $h_{\rm cut}=5.5$ Å up to about 10 Å, after which it starts deviating. This deviation is understandable; with this cutoff, a quarter of the droplet is excluded from the fit.

After validating the approach with average droplet surfaces and instantaneous out-of-equilibrium configuration, we turn to the droplet dynamics. As we have already mentioned, one of the most appealing features of this approach is that having access to instantaneous configurations of the surface molecules allows us to track the time evolution of the contact angle and other geometric parameters. As a first example, we start from the compressed cylindrical droplet used for the previous calculation and release the downward acceleration, allowing the droplet to relax back to its equilibrium shape. In Fig. 5 (top panel), we report the time evolution of the left and right contact angles from the moment the downward acceleration is removed, averaging over a running window of 8 frames for clarity. This allows also to estimate the statistical error on the reported quantities. Both contact angles show an initial relaxation that is followed by, and partially masked by, large os-

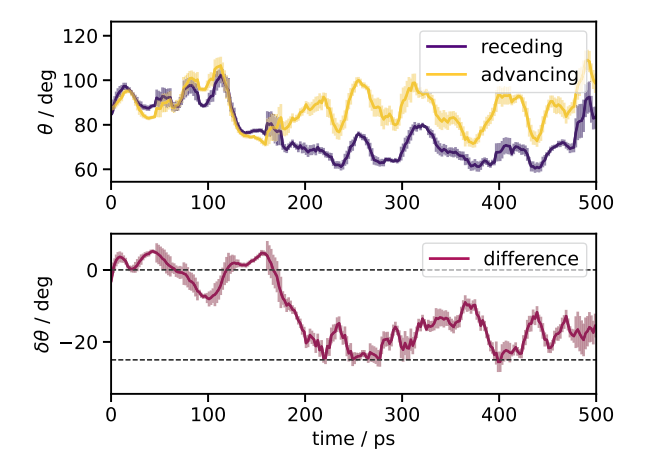


Fig. 6. Time evolution of the receding (lower stationary values) and advancing (higher stationary values) contact angles in a droplet subjected to lateral acceleration. The shaded area represents one standard deviation.

cillations. The eccentricity $\epsilon = \sqrt{1 - (m/M)^2}$, where m and M lengths of the minor and major semiaxes, is another geometrical parameter of the ellipse, which can be used to characterize its deformation. We show the evolution of the eccentricity over time in the bottom panel of Fig. 5.

Next, we apply our approach to exploring the evolution of contact angles of the cylindrical droplet in response to a lateral body force by applying a constant acceleration of 0.0015 nm/ps^2 along the x axis. We characterize the droplet's response by the evolution of its advancing and receding contact angles over time, as shown in Fig. 6. The initial stage is characterized by a symmetric response of the droplet, with both advancing and receding contact angles evolving in lockstep up to about 150 ps. At later times, the two angles quickly diverge to start fluctuating around their respective stationary values of about 70 and 95 deg.

As the force is switched on instantaneously and is rather strong, the droplet is initially (0-150 ps) characterized by a large slip velocity and moves almost by uniform translation (evident by visual inspection of the trajectory). When the initial shock relaxes, and the wall friction starts becoming effective, slip reduces, but it takes additional time for momentum to be transported by viscous dissipation, giving rise to the transition region seen in the lower panel between 150-200 ps, followed by the stationary state beyond 200 ps.

The transition region is better underlined by looking at the difference between the values of the two instantaneous contact angles, shown in the bottom panel of Fig. 6 that oscillates at first around zero, and after a quick transition phase, around about -25 deg.

We now apply the method in the case of a droplet made of the same number of molecules but placed on a larger substrate. This way, the droplet does not span the periodic boundary conditions in any direction, and its equilibrium shape is that of a spherical cap. We impose to each water molecule an acceleration in the x-z plane of [0.007,0.0,0.004] nm/ps², effectively inducing a motion along the x axis combined with a stretching of the droplet, which is also pulled along the vertical z axis. The stationary shape of the droplet, shown in the bottom panel of Fig. 1, is that of a tilted ellipsoid. Using the conventional approach, the absence of any symmetry would require extensive sampling to locate the interface in the three-dimensional space. In Fig. 7, instead, we show the result of the nonlinear ellipsoidal fit to a single configuration, which yielded an RMSD of 2.75 Å. As usual, we did not include the molecules in the first layer in contact with the substrate, retaining only molecules farther than 5.5 Å.

Access to the best-fit ellipsoid allows computing the contact line location and the contact angle value along it, as described in the Methods section. The contact angle can be conveniently expressed as a function of the azimuthal angle ϕ . If we set the origin of the (x,y) coordinate system in the center of the droplet, then $\phi=0$ corresponds to the foremost point of the advancing contact line (for a droplet that advances towards

larger values of x), while $\phi = \pm \pi$ correspond to the back of the moving droplet. We report the contact angle as a function of the azimuthal one in Fig. 8. The contact angle is minimum and slightly larger than 100 deg close to the back of the droplet, as it is also evident from the right panel of Fig. 7, and then reaches the maximum value close, about 114 deg close to the advancing front. Note that the graph is very smooth because the contact angle is an analytical function of the azimuthal one.

As a general remark, in all three cases the droplets behave quite in similar ways, and beside the reported measurements it is worth mentioning the clear appearance of higher modes, which are of course not captured with the current approach, as well as the Noether mode [47, 54], which entails a constant velocity translation of the droplet, this one detectable with our approach as it gives rise to a tilted ellipse/ellipsoid. Interestingly, and contrarily to our initial expectations, the ellipsoidal fit seemed to be more stable than the elliptical one under small perturbations of the system.

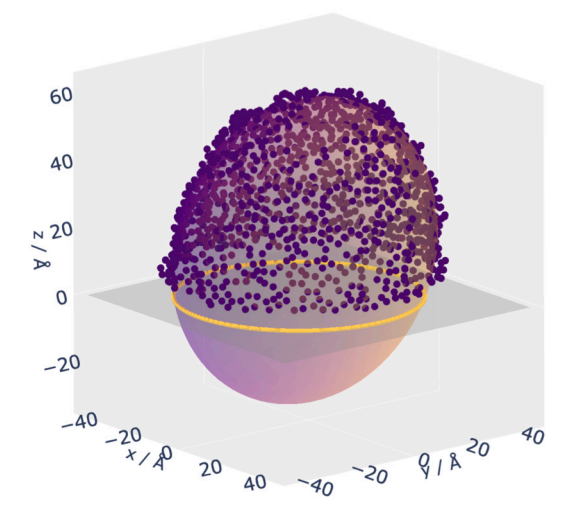
Finally, we want to compare more traditional approaches based on the location of the interface via the density profile and the present one. The single-frame calculation is often impossible when using approaches based on sampling the density profile because of the sheer lack of statistics. However, it is possible to compare the results at equilibrium or in a stationary state, where it is possible to perform extensive sampling. Here, we opted to compare the location of the interface of the equilibrium cylindrical droplet with the present method. Instead of computing the locus of an arbitrary isodensity value, we performed a fit to the function

$$\rho(r;h) = \rho(h)\frac{1}{2}\left[1 - \tanh\left(\frac{r - r_{\text{inter}}(h)}{w(h)}\right)\right],\tag{7}$$

using $r_{\text{inter}}(h)$, w(h) and $\rho(h)$ as fitting parameters for different slices at constant elevation h, and used $r_{inter}(h)$ as a proxy to the location of the interface. More refined approaches could use the sampled density profile to compute, for example, the location of the Gibbs equimolar dividing surface. In Fig. 9, we compare this way of estimating the interface location and the one based on the average location of the surface atoms as identified by GITIM, using 100 frames of an equilibrium simulation. The two profiles compare rather well, even though they appear to have a slightly different radius. This difference is unsurprising, as both approaches use a free parameter, namely the probe sphere radius for GITIM and the choice of the midpoint of the tanh function for the traditional approach. However, the traditional approach suffers from additional sampling problems next to the tip of the droplet, where it does not make sense anymore to fit a sigmoidal density profile. In this case, it would be more appropriate to sample the density as a function of the radial distance from the droplet base center and the corresponding polar angle. Regardless of these discrepancies, the two approaches provide overall qualitatively consistent profiles. Note that with the traditional approach there would be not enough statistics to perform a density profile fit from a single frame, and long sampling is needed, which could prevent analysis of the droplet shape in non-stationary conditions.

4. Conclusions

Accessing the geometric information from instantaneous configurations of droplets in computer simulations can improve our understanding of the effect of substrate-liquid interactions and fluid additives on the short-time response of droplets. The availability of this information can impact applications like coating, inkjet printing technologies, and smart surfaces, as well as our fundamental understanding of environmentally relevant processes involving, for example, aerosols. In addition, recent developments in interferometric and spectroscopic techniques (see, for example, Refs. [55–57]) are providing access to the static and dynamics of interfacial layers in the 1-100 nm range, and molecular dynamics simulations can supply a complementary point of view after subtracting the smearing effect of high-frequency capillary



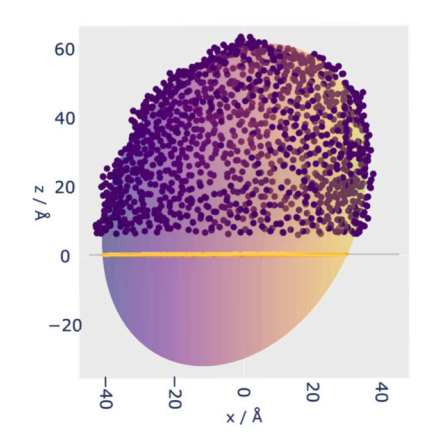


Fig. 7. Instantaneous configuration of the oxygen atoms in the spherical droplet pulled by an oblique body force (points) and best-fitting ellipsoid (smooth surface). Left: oblique projection; Right: side view. Only the atoms used for the fit are shown. The contact line is also shown in yellow at the intersection between the ellipsoid and the plane of the substrate. This fit yielded an RMSD of 2.75 Å.

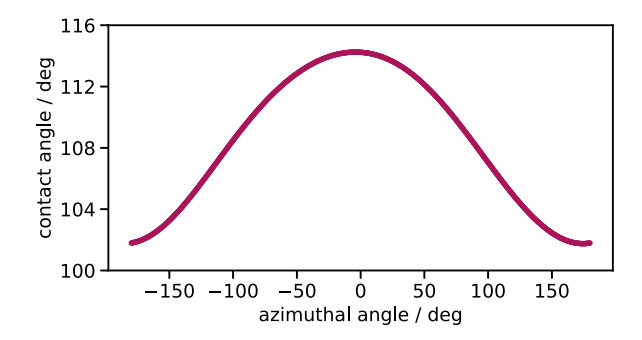


Fig. 8. Contact angle along the contact line of the best-fitting ellipsoid. The azimuthal angle is zero for the most advanced point of the contact line, along the positive x semiaxis (with the origin in the center of the droplet) and ± 180 deg along the negative x semiaxis.

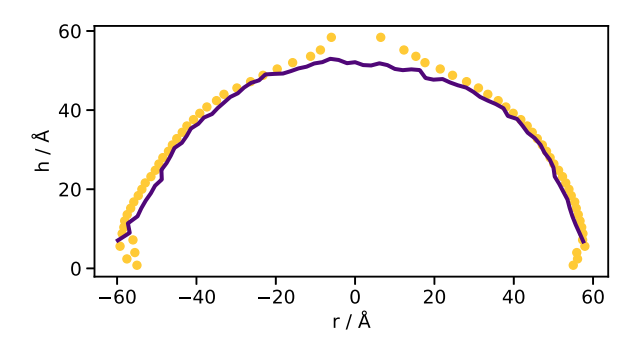


Fig. 9. Comparison between the average location of the interfacial atoms computed using the GITIM algorithm (continuous line) and the interface location r_{inter} computed by fitting the density profile (points).

waves. In this work, we present a computational framework for measuring instantaneous contact angles of liquid droplets based on algorithms for identifying surface molecules and introduce a robust ellipse-fitting procedure to model the first excited modes. The case studies presented here emphasize our approach's ability to track the time evolution of the surface of droplets, including the deformation of the global shape induced by thermal fluctuations.

CRediT authorship contribution statement

Amal Kanta Giri: Writing – review & editing, Validation, Software, Investigation. Marcello Sega: Writing – original draft, Supervision, Software, Project administration, Methodology, Funding acquisition, Conceptualization.

Declaration of competing interest

The authors declare that they have no known competing financial interests or personal relationships that could have appeared to influence the work reported in this paper.

Data availability

Data will be made available on request.

Acknowledgements

The authors acknowledge funding by the German Research Foundation (DFG) through project #422794127 within the DFG Priority Program SPP 2171 Dynamic Wetting of Flexible, Adaptive, and Switchable Substrates.

References

- T. Huhtamäki, X. Tian, J.T. Korhonen, R.H. Ras, Surface-wetting characterization using contact-angle measurements, Nat. Protoc. 13 (7) (2018) 1521–1538.
- [2] C.D. Volpe, S. Siboni, The Wilhelmy method: a critical and practical review, Surf. Innov. 6 (3) (2018) 120–132.
- [3] G. Saville, Computer simulation of the liquid-solid-vapour contact angle, J. Chem. Soc. Faraday Trans. II 73 (7) (1977) 1122–1132.
- [4] J. Koplik, J.R. Banavar, J.F. Willemsen, Molecular dynamics of fluid flow at solid surfaces, Phys. Fluids A, Fluid Dyn. 1 (5) (1989) 781–794.
- [5] P.A. Thompson, M.O. Robbins, Simulations of contact-line motion: slip and the dynamic contact angle, Phys. Rev. Lett. 63 (7) (1989) 766.
- [6] E. Bertrand, T.D. Blake, J. De Coninck, Influence of solid-liquid interactions on dynamic wetting: a molecular dynamics study, J. Phys. Condens. Matter 21 (46) (2009) 464124.
- [7] A.V. Lukyanov, A.E. Likhtman, Dynamic contact angle at the nanoscale: a unified view, ACS Nano 10 (6) (2016) 6045–6053.
- [8] M. Kanduč, L. Eixeres, S. Liese, R.R. Netz, Generalized line tension of water nanodroplets, Phys. Rev. E 98 (3) (2018) 032804.
- [9] L. Boruvka, A. Neumann, Generalization of the classical theory of capillarity, J. Chem. Phys. 66 (12) (1977) 5464–5476.
- [10] J.S. Rowlinson, B. Widom, Molecular Theory of Capillarity, Dover Publications, Inc., Mineola, New York, 1982.

- [11] B. Andreotti, J.H. Snoeijer, Statics and dynamics of soft wetting, Annu. Rev. Fluid Mech. 52 (2020) 285–308.
- [12] M. Vuckovac, M. Latikka, K. Liu, T. Huhtamäki, R.H. Ras, Uncertainties in contact angle goniometry, Soft Matter 15 (35) (2019) 7089–7096.
- [13] H. Jiang, A.J. Patel, Recent advances in estimating contact angles using molecular simulations and enhanced sampling methods, Curr. Opin. Chem. Eng. 23 (2019) 130–137.
- [14] H. Jiang, F. Müller-Plathe, A.Z. Panagiotopoulos, Contact angles from Young's equation in molecular dynamics simulations, J. Chem. Phys. 147 (8) (2017).
- [15] J. Zhang, P. Wang, M.K. Borg, J.M. Reese, D. Wen, A critical assessment of the line tension determined by the modified Young's equation, Phys. Fluids 30 (8) (2018).
- [16] F. Pizzitutti, M. Marchi, F. Sterpone, P.J. Rossky, How protein surfaces induce anomalous dynamics of hydration water, J. Phys. Chem. B 111 (26) (2007) 7584–7590
- [17] H. Li, X.C. Zeng, Wetting and interfacial properties of water nanodroplets in contact with graphene and monolayer boron-nitride sheets, ACS Nano 6 (3) (2012) 2401–2409.
- [18] E.E. Santiso, C. Herdes, E.A. Müller, On the calculation of solid-fluid contact angles from molecular dynamics, Entropy 15 (9) (2013) 3734–3745.
- [19] A. Braslau, P.S. Pershan, G. Swislow, B. Ocko, J. Als-Nielsen, Capillary waves on the surface of simple liquids measured by X-ray reflectivity, Phys. Rev. A 38 (5) (1988) 2457
- [20] E. Chacón, P. Tarazona, Intrinsic profiles beyond the capillary wave theory: a Monte Carlo study, Phys. Rev. Lett. 91 (16) (2003) 166103, https://doi.org/10.1103/ PhysRevLett.91.166103.
- [21] J. Škvára, J. Škvor, I. Nezbeda, Evaluation of the contact angle from molecular simulations, Mol. Simul. 44 (3) (2018) 190–199.
- [22] S. Ravipati, B. Aymard, S. Kalliadasis, A. Galindo, On the equilibrium contact angle of sessile liquid drops from molecular dynamics simulations, J. Chem. Phys. 148 (16) (2018) 164704.
- [23] A.P. Willard, D. Chandler, Instantaneous liquid interfaces, J. Phys. Chem. B 114 (5) (2010) 1954–1958.
- [24] M. Sega, S.S. Kantorovich, P. Jedlovszky, M. Jorge, The generalized identification of truly interfacial molecules (itim) algorithm for nonplanar interfaces, J. Chem. Phys. 138 (4) (2013), https://doi.org/10.1063/1.4776196.
- [25] M. Sega, G. Hantal, B. Fábián, P. Jedlovszky, Pytim: a python package for the interfacial analysis of molecular simulations, J. Comput. Chem. (2018), https:// doi.org/10.1002/jcc.25384.
- [26] A.K. Giri, P. Malgaretti, D. Peschka, M. Sega, Resolving the microscopic hydrodynamics at the moving contact line, Phys. Rev. Fluids 7 (10) (2022) L102001, https:// doi.org/10.1103/PhysRevFluids.7.L102001.
- [27] H.J.C. Berendsen, J.R. Grigera, T.P. Straatsma, The missing term in effective pair potentials, J. Phys. Chem. 91 (24) (1987) 6269–6271, https://doi.org/10.1021/ j100308a038.
- [28] S. Miyamoto, P.A. Kollman, Settle: an analytical version of the SHAKE and RATTLE algorithm for rigid water models, J. Comput. Chem. 13 (8) (1992) 952–962.
- [29] M. Sega, M. Sbragaglia, L. Biferale, S. Succi, Regularization of the slip length divergence in water nanoflows by inhomogeneities at the Angstrom scale, Soft Matter 9 (35) (2013) 8526–8531, https://doi.org/10.1039/C3SM51508G.
- [30] P.A. Thompson, S.M. Troian, A general boundary condition for liquid flow at solid surfaces, Nature 389 (6649) (1997) 360–362, https://doi.org/10.1038/38686.
- [31] A. Kozbial, C. Trouba, H. Liu, L. Li, Characterization of the intrinsic water wettability of graphite using contact angle measurements: effect of defects on static and dynamic contact angles, Langmuir 33 (4) (2017) 959–967.
- [32] A. Méndez-Vilas, A.B. Jódar-Reyes, M.L. González-Martín, Ultrasmall liquid droplets on solid surfaces: production, imaging, and relevance for current wetting research, Small 5 (12) (2009) 1366–1390.
- [33] G. Scocchi, D. Sergi, C. D'Angelo, A. Ortona, Wetting and contact-line effects for spherical and cylindrical droplets on graphene layers: a comparative moleculardynamics investigation, Phys. Rev. E 84 (6) (2011) 061602.

- [34] M.J. Abraham, T. Murtola, R. Schulz, S. Páll, J.C. Smith, B. Hess, E. Lindahl, GROMACS: high performance molecular simulations through multi-level parallelism from laptops to supercomputers, SoftwareX 1–2 (2015) 19–25, https:// doi.org/10.1016/j.softx.2015.06.001.
- [35] U. Essmann, L. Perera, M.L. Berkowitz, T. Darden, H. Lee, L.G. Pedersen, A smooth particle mesh Ewald method, J. Chem. Phys. 103 (19) (1995) 8577–8593, https://doi.org/10.1063/1.470117.
- [36] C.L. Wennberg, T. Murtola, S. Páll, M.J. Abraham, B. Hess, E. Lindahl, Direct-space corrections enable fast and accurate Lorentz–Berthelot combination rule Lennard-Jones lattice summation, J. Chem. Theory Comput. 11 (12) (2015) 5737–5746.
- [37] A.E. Ismail, G.S. Grest, M.J. Stevens, Capillary waves at the liquid-vapor interface and the surface tension of water, J. Chem. Phys. 125 (1) (2006).
- [38] M. Sega, C. Dellago, Long-range dispersion effects on the water/vapor interface simulated using the most common models, J. Phys. Chem. B 121 (15) (2017) 3798–3803, https://doi.org/10.1021/acs.jpcb.6b12437.
- [39] S. Nosé, A molecular dynamics method for simulations in the canonical ensemble, Mol. Phys. 52 (2) (1984) 255–268.
- [40] W.G. Hoover, Canonical dynamics: equilibrium phase-space distributions, Phys. Rev. A 31 (3) (1985) 1695.
- [41] M. Sega, P. Jedlovszky, The impact of tensorial temperature on equilibrium thermodynamics, Phys. Chem. Chem. Phys. 20 (25) (2018) 16910–16912, https:// doi.org/10.1039/C8CP02046A.
- [42] M. Sega, B. Fábian, P. Jedlovszky, Nonzero ideal gas contribution to the surface tension of water, J. Phys. Chem. Lett. 8 (12) (2017) 2608–2612, https://doi.org/10. 1021/acs.jpclett.7b01024.
- [43] B. Delaunay, Sur la sphere vide, Izv. Akad. Nauk SSSR 7 (793-800) (1934) 1-2.
- [44] G. Hantal, P. Jedlovszky, M. Sega, Local structure of liquid/vapour interfaces approaching the critical point, Soft Matter 19 (21) (2023) 3773–3782.
- [45] F.A. Dahlen, J. Tromp, Spheroidal and toroidal oscillations, in: Theoretical Global Seismology, Princeton University Press, 1998.
- [46] H. Lamb, Hydrodynamics, The University Press, 1932.
- [47] J. Bostwick, P. Steen, Dynamics of sessile drops. Part 1. Inviscid theory, J. Fluid Mech. 760 (2014) 5–38.
- [48] P. Maffettone, M. Minale, Equation of change for ellipsoidal drops in viscous flow, J. Non-Newton. Fluid Mech. 78 (2–3) (1998) 227–241.
- [49] N.E. Jackson, C.L. Tucker III, A model for large deformation of an ellipsoidal droplet with interfacial tension, J. Rheol. 47 (3) (2003) 659–682.
- [50] A. Fitzgibbon, M. Pilu, R.B. Fisher, Direct least square fitting of ellipses, IEEE Trans. Pattern Anal. Mach. Intell. 21 (5) (1999) 476–480.
- [51] R. Halır, J. Flusser, Numerically stable direct least squares fitting of ellipses, in: Proc. 6th International Conference in Central Europe on Computer Graphics and Visualization, in: WSCG, vol. 98, Citeseer, 1998, pp. 125–132.
- [52] D. Turner, I. Anderson, J. Mason, M. Cox, An algorithm for fitting an ellipsoid to data, Tech. Rep., National Physical Laboratory, UK, 1999, http://citeseerx.ist.psu. edu/viewdoc/summary?doi=10.1.1.36.2773.
- [53] M. Grötschel, L. Lovász, A. Schrijver, Geometric Algorithms and Combinatorial Optimization, vol. 2, Springer Science & Business Media, 2012.
- [54] D. Lyubimov, T. Lyubimova, S. Shklyaev, Non-axisymmetric oscillations of a hemispherical drop, Fluid Dyn. 39 (6) (2004) 851–862.
- [55] M. Corti, A. Raudino, L. Cantu', J. Theisen, M. Pleines, T. Zemb, Nanometric surface oscillation spectroscopy of water-poor microemulsions, Langmuir 34 (28) (2018) 8154–8162, https://doi.org/10.1021/acs.langmuir.8b00716.
- [56] F. Tang, T. Ohto, S. Sun, J.R. Rouxel, S. Imoto, E.H.G. Backus, S. Mukamel, M. Bonn, Y. Nagata, Molecular structure and modeling of water-air and ice-air interfaces monitored by sum-frequency generation, Chem. Rev. 120 (8) (2020) 3633–3667, https://doi.org/10.1021/acs.chemrev.9b00512.
- [57] Y. Litman, K.-Y. Chiang, T. Seki, Y. Nagata, M. Bonn, Surface stratification determines the interfacial water structure of simple electrolyte solutions, Nat. Chem. (2024) 1–7, https://doi.org/10.1038/s41557-023-01416-6.